ISIS-I AND ISIS-II OBSERVATION OF EMISSIONS TRIGGERED BY DOPPLER-SHIFTED NORWAY OMEGA SIGNALS

Toshio MATSUO[1], Iwane KIMURA[1] and Hisao YAMAGISHI[2]

[1]*Department of Electrical Engineering, Kyoto University, Yoshida Honmachi, Sakyo-ku, Kyoto 606*
[2]*National Institute of Polar Research, 9–10, Kaga 1-chome, Itabashi-ku, Tokyo 173*

Abstract: A great number of VLF spectra were collected by receiving the telemetry of ISIS satellites at Syowa Station, Antarctica, for about 6 years from May 1976 to February 1982. Norway Omega signals propagated in the non-ducted mode to the southern hemisphere and observed by the polar orbiting ISIS-I and ISIS-II satellites have shown very interesting latitudinal characteristics of their positive and negative doppler shift. According to EDGAR (J. Geophys. Res., **81**, 3327, 1976), these characteristics are explicable by taking into account the wave normal direction at the satellite location, which can be estimated from the results of ray tracing. One very important result of our observation is that VLF emissions triggered by positively and negatively doppler-shifted Omega signals were discovered. From the doppler frequency shift of the triggering signal, we can determine their wave normal direction at the satellite as mentioned above, so that we have further tried to estimate their wave normal direction in the interaction region near the equatorial plane, where the triggered emissions are thought to have been generated. One such estimation for the case observed on November 28, 1979 results in the wave normal angles at the equatorial plane to be around 10°–30°. Furthermore, in other Omega data, it can be shown that the wave normal angles for large doppler-shifted signals approach about 40°–60° at $L<2.7$.

1. Introduction

VLF signals injected from the ground-based transmitters have been used as an effective means to study wave propagation characteristics and wave particle interaction phenomena in the magnetosphere. CARPENTER *et al.* (1969) reported that magnetospheric noise was triggered by NAA (17.8 kHz), when the minimum gyrofrequency on the ray path became twice the NAA frequency. In addition, both triggering waves and associated triggered emissions were thought to have traveled to the conjugate points along whistler mode ducts. As only VLF waves propagating from the opposite hemisphere through the ionization ducts can penetrate the ionosphere and can reach the ground, it has been believed that the triggered waves observed on the ground must have propagated along the ducts (*e.g.*, HELLIWELL and KATSUFRAKIS, 1974; CARPENTER and MILLER, 1976). The wave normal direction of the triggering waves in the interaction region around the geomagnetic equator is thought to be nearly parallel to the geomagnetic field line, and this condition has been a theoretical basis for the wave particle interaction for VLF emission generation. To the contrary, even if triggered emissions might be generated by non-ducted VLF signals, these emissions and trig-

gering signals cannot be observed on the ground, because these waves cannot penetrate the ionosphere due to their large wave normal angles. In satellite observations, there are many examples of detection of non-ducted signals evidenced by their large doppler shift. For example, WALTER and ANGERAMI (1969) reported that a ground-based signal observed on the OGO-4 satellite exhibits the characteristics of doppler shift. CERISIER (1973, 1974), KOONS *et al.* (1974), and EDGAR (1976) showed latitudinal variation characteristics of the doppler shift of ground-based signals observed over a wide latitudinal range. Especially, EDGAR (1976) explained this characteristic by ray tracing using his special electron density profile with a latitudinal dependence of the ionospheric electron density. Wave normal directions for Norway Omega signals observed by the GEOS-1 satellite were analyzed by using the concept of wave distribution function (NEUBERT *et al.*, 1983; LEFEUVRE *et al.*, 1982). In these papers, no description was given on the triggered emissions associated with the non-ducted signals. BELL *et al.* (1981) first pointed out that emissions observed on the satellite were triggered at the tail of prolonged signals, and from this phenomenon he concluded that the emissions were triggered by signals, which are thought to be in non-ducted propagation. But, up to the present, no one has discussed in detail the wave normal angles of the triggering waves for emissions in the generation region.

2. Ground and Satellite Observation of Omega Signals

Since a satellite telemetry receiving system for the purpose of data acquisition of VLF spectrograms observed by satellites in the polar region was installed at Syowa Station (69.1°S, 39.6°E geographic, 70.03°S, 79.39°E geomagnetic), we have tracked 962 passes of the polar orbiting satellites ISIS-I (570–3520 km) and ISIS-II (~1400 km) for about 6 years from May 1976 to January 1982. On these satellites, dipole antennas are connected to the VLF (0.05–27 kHz) receiver. Among the VLF spectrograms obtained, we could find the Omega signals transmitted from Aldra, Norway (66.25°N, 13.09°E geographic) in 150 passes out of total 962 passes. However, triggered emissions due to these signals were detected only in 23 out of 150 passes. Statistical features of the observed Omega signals were already reported in detail by MATSUO *et al.* (1983).

As is well known, Omega signals transmitted from 8 stations in the world have been used to determine the location of ship by making use of the stable propagation characteristics in long distances. Leading edges of 10.2 kHz Omega pulses transmitted in 1979 from Aldra, Norway correspond to 2, 12, 22 s, etc., as shown in Fig. 1a, and the figure also shows the time sequence of the Norway Omega transmissions at frequencies 10.2, 13.6, 11.33, 12.1, 12.1, 11.05, 12.1 and 12.1 kHz respectively, with specified signal lengths according to the Omega signal format. All the transmitted pulses in the same or different frequencies are spaced by 0.2 s.

Figure 2 shows spectrograms of Norway Omega signals and associated triggered emissions observed by ISIS-II satellite on November 28, 1979 in the southern hemisphere. Omega signals in the frequency range from about 10 to 14 kHz are seen successively. The emissions triggered by the 10.2 kHz signals are strongly observed over the wide region from $L=2.4$ to nearly $L=6$, but emissions by the signals of other frequencies

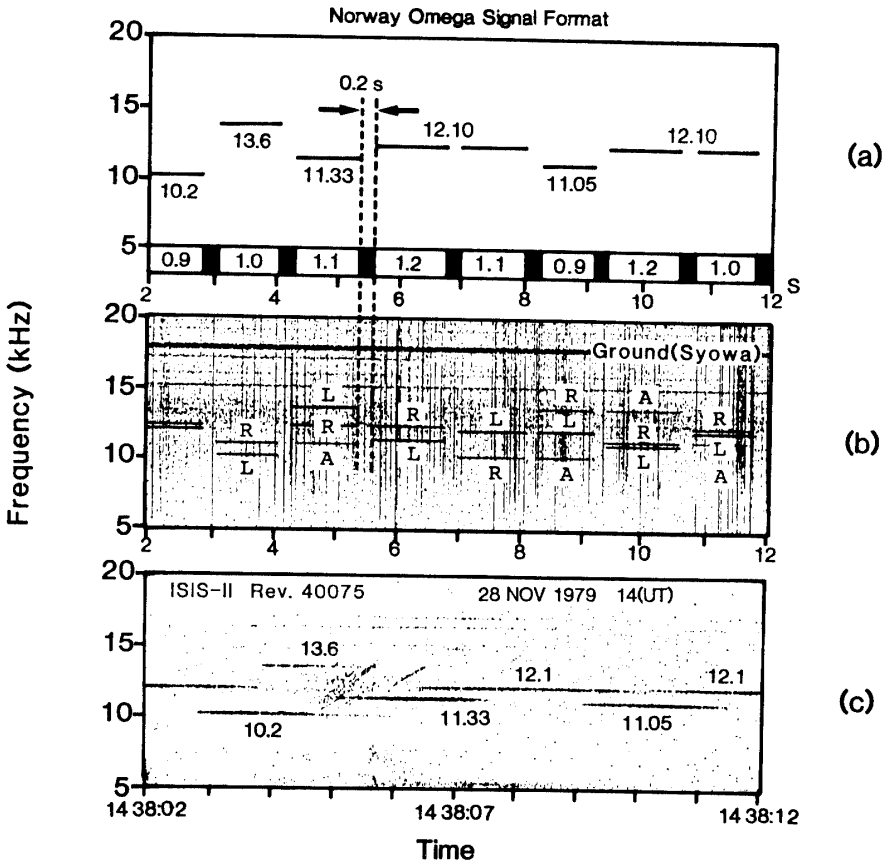

Fig. 1. (*a*) *Transmission frequency format of Norway Omega signal. Leading edges of 10.2 kHz pulse in 1979 are 2, 12, 22 s, etc, and this format is repeated every 10 s. Pulse lengths are in the range 0.9–1.2 s.*
(*b*) *Reunion* (*R*), *Liberia* (*L*) *and Argentina* (*A*) *Omega signals are observed at Syowa Station, but signals from Norway are not observed.*
(*c*) *Prolonged Omega signals and associated triggered emissions observed on the ISIS-II satellite on November 28, 1979. A 10.2 kHz signal transmitted from Aldra on 1438: 02 UT is observed after a time delay of about 1 s on the ISIS-II satellite in the southern hemisphere due to a propagation time.*

are faintly seen.

Figure 1b shows the frequency-spectrograms of Omega signals which were also simultaneously observed on the ground at Syowa Station, where Omega signals transmitted from Reunion, Liberia and Argentina can be detected by the waveguide propagation mode between the ground and the ionosphere. These signals are clearly identified by referring to the Omega signal format assigned to each station. It is shown that each signal is never overlapped in time with those from other stations, and Norway Omega signals have never been observed at Syowa Station, because of the long distance from the source. On the other hand, most of signals observed by ISIS are Norway Omega signals, but Reunion (20.58°S, 55.17°E geographic) Omega signals have been rarely observed by ISIS even in the vicinity of the transmitter.

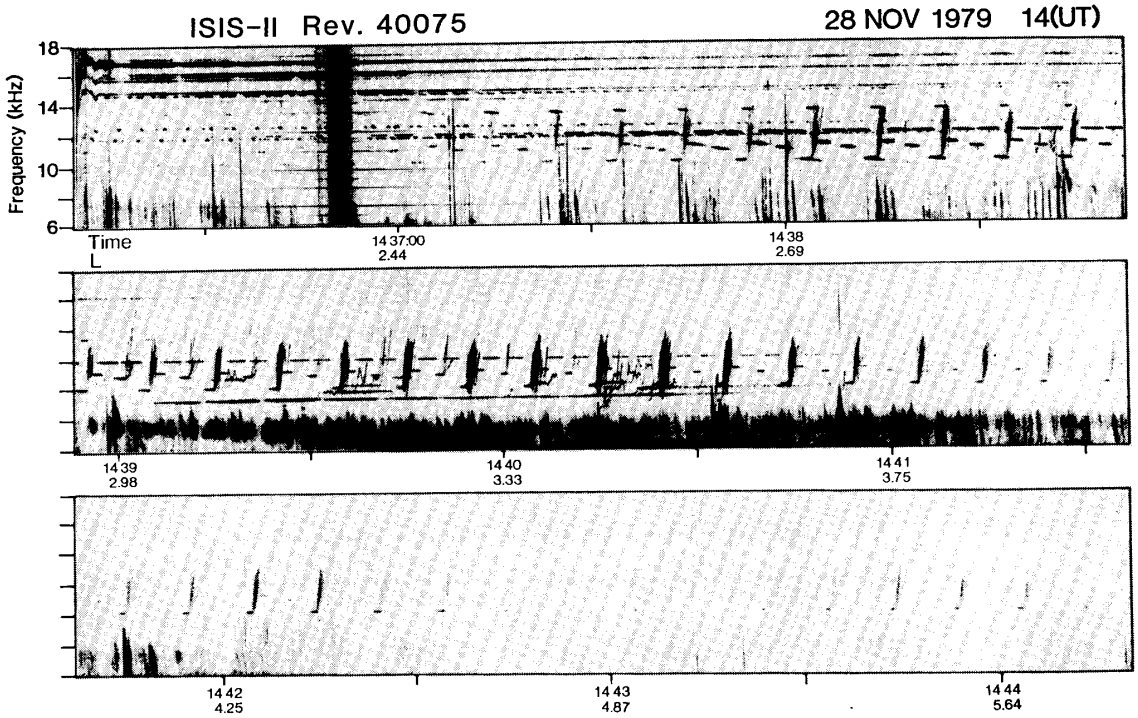

Fig. 2. Frequency-time spectrogram observed on the ISIS-II satellite on November 28, 1979. Omega signals in the frequency range 10.2–13.6 kHz and triggered emissions are observed during the interval from nearly $L=2.4$ to $L=6$ in most of the time, and the emissions seemed to be triggered strongly by 10.2 kHz signals.

3. Prolongation and Doppler Shift

Figure 1c shows a representative spectrum observed by ISIS-II of Omega signals which propagated in a whistler mode from Norway. Although all the transmitted pulses are regularly spaced by 200 ms, Norway Omega pulses observed by ISIS near Syowa Station are clearly longer than the original pulse lengths as compared with Fig. 1a. Such a prolongation of Norway Omega signals is a very common phenomenon in the ISIS satellite observations. Especially, one interesting feature is that the pulse length of the 10.2 kHz signals increases with increasing latitude, and it becomes maximum at nearly $L=2.7$. After passing this point, it decreases gradually to the original transmitted pulse length. In order to investigate the cause of such prolongation characteristics, frequency-expanded spectrograms were made around the Omega frequency.

Figure 3 shows a frequency-time spectrogram expanded at a selected frequency band including the 11.05 and 11.33 kHz signals. It is evident from the figure that both signals are composed of several isolated pulses whose frequencies and arrival times are different from each other. This feature implies that each isolated pulse has arrived at the satellite with a different wave normal direction, so that their arrival time and doppler frequency shift become different from each other. The doppler shift can be positive when the direction of satellite movement and the direction of the wave normal are opposite and be negative when these two are in the same direction. Ac-

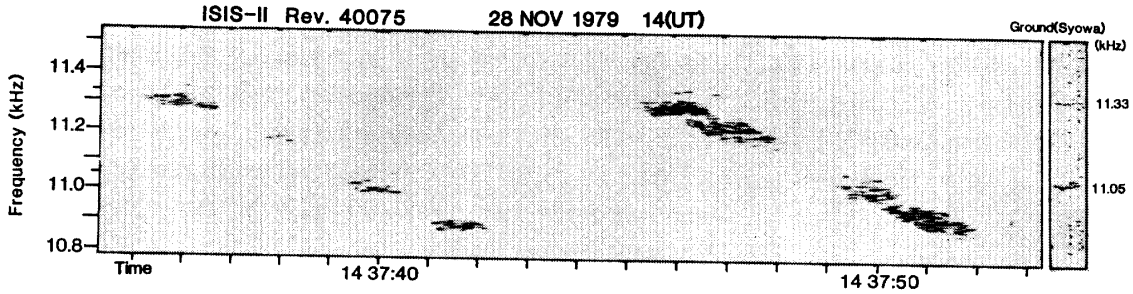

Fig. 3. Expanded spectrogram of Norway Omega signal observed on the ISIS-II satellite on November 28, 1979 is showing that the observed signals (at 11.05 and 11.33 kHz) are composed of several different doppler-shifted components. It is possible to distinguish a slightly positive doppler-shifted component from several large negative doppler-shifted signals in comparison with 11.05 and 11.33 kHz Reunion Omega signals observed at Syowa Station as shown in the right side spectrogram.

tually on the satellite both negative and positive doppler-shifted components are observed at the same time. This means that there are components with a variety of wave normal directions at the satellite.

If the time scale is shortened, frequency scale-expanded spectra for 10.2 kHz signals observed by ISIS-II moving toward a higher L region appear as shown in Fig. 4. It is very clear from this figure that both positive and negative doppler-shifted components are seen from $L=2.4$ to nearly 6. The detailed characteristics of the doppler shift are as follows:

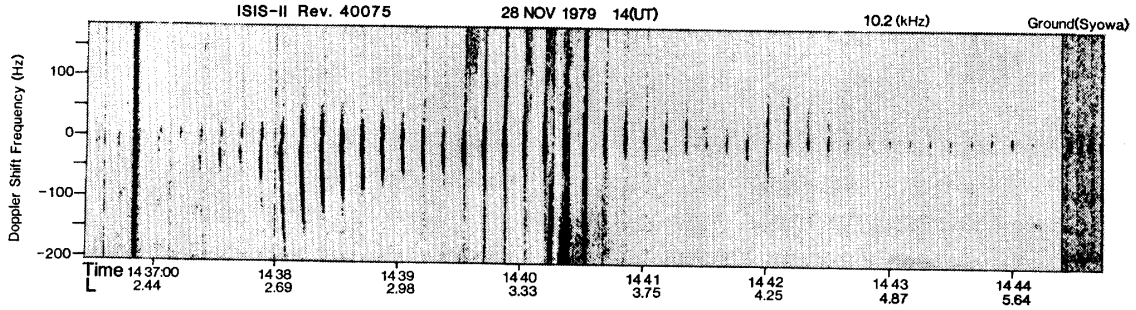

Fig. 4. Time scale shortened and frequency scale expanded spectrogram showing representative latitudinal characteristics of doppler shift frequency observed on November 28, 1979 when ISIS-II moved from the equatorward to the southpole. Positive and negative doppler-shifted signals were observed by ISIS-II moving southward. Right side spectrogram shows the spectra of 10.2 kHz Reunion and Liberia Omega signals observed on the ground (Syowa Station).

(1) A large negative doppler-shifted component is observed over a wide latitudinal range from $L=2.4$ to nearly 4. The negative doppler shift increases with increasing satellite L value from $L=2.4$ to 2.7 and it reaches a maximum value of 170 Hz. Once ISIS-II has passed over this L value, the doppler shift decreases gradually, and the observed frequency becomes almost equal to the transmitted frequency.

(2) The magnitude of the positive doppler shift is smaller than that of the negative doppler shift, but the latitudinal variation rate of the positive doppler shift is similar to that of the negative one.

(3) If the satellite moves from the south to the equator, the characteristics of the polarity and the magnitude of doppler shift are reversed as expected. Actually, when the ISIS-I moved equatorward from the south pole, the doppler shift was always positive and the magnitude of positive doppler shift was always greater than those of negative for $L<2.6$ (such spectra are shown in Figs. 15b and 15c). This fact supports our hypothesis that the frequency-expanded spectra of the Omega Norway signals are attributed to the doppler shifts for multiple ray paths.

As is well known, the doppler shift observed by a moving satellite in a space plasma is indicated by the following formula.

$$\Delta f = -\frac{f}{c} \cdot n \cdot V \cdot \cos \delta ,$$

where f is the frequency of signal, c is the light velocity in vacuum, n is the phase refractive index, V is the satellite velocity, and δ is the angle between the wave normal direction and the satellite velocity vector. The magnitude of doppler shift depends mainly upon n which is governed by the electron density, the cyclotron frequency and the wave normal angle relative to the direction of the geomagnetic field. We first estimate the amount of doppler shift to be observed by the satellite under the assumption that the Norway Omega signals propagate to the satellites along an ionization duct from the source location. The calculated doppler shift amounts to several Hz at the largest. However, the doppler shifts actually observed amount to 170 Hz, as shown in Fig. 4. This fact implies that the wave normal angles must have approached the resonance cone angle.

4. Wave Normal Angles of Triggering Waves

Since the magnitude and the polarity of doppler shift frequency provide wave normal direction of the signal with respect to the earth's magnetic field B_0, this direction may be used as the initial wave normal angle in tracing the ray path of the Omega signal by the backward ray tracing technique based on a centered dipole field model on an assumed electron density model (KIMURA, 1966). In the following, however, we calculate the ray paths starting from different entrance latitudes near Aldra, Norway in the northern hemisphere, and calculate the doppler shift for the ray paths at the satellite in the southern hemisphere. Thus for each location of the satellite, a latitudinal variation characteristic of the doppler shift frequency can be constructed.

As was pointed out by EDGAR (1976), an electron density profile based on the diffusive equilibrium model, in which the electron density at the reference level decreases with increasing latitudes for $2<L<3$, is required to explain a latitudinal doppler shift characteristic for a VLF signal transmitted from Alaska ($L=4$, 13.275 kHz, Aerospace Corp.) and FUB (16.8 kHz) signal actually observed by ISIS-II and FR-1 satellites respectively. We have also utilized similar electron density models with variable latitudinal gradients of electron density at the reference level. The most appropriate model to fit our observed data is shown in Fig. 5, where the plasmapause location and magnetospheric cold plasma density gradient are thought to be located around $L=4.2$ and 3.5 respectively. This cold plasma density model is constructed

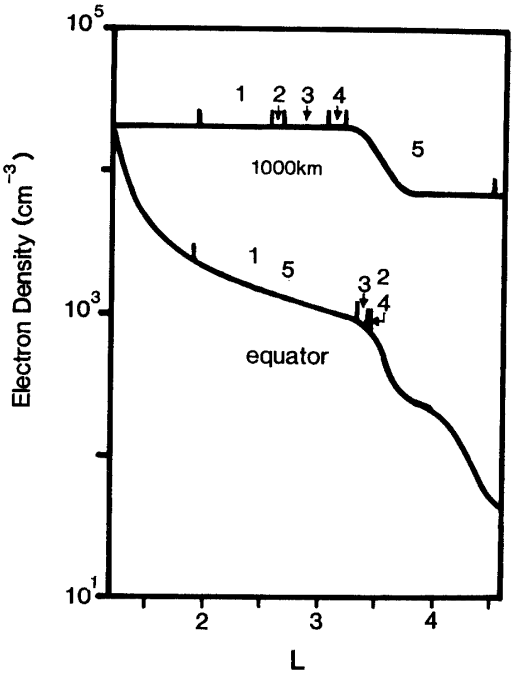

Fig. 5. Equatorial electron density model used in calculation of ray paths for $L<4.2$. The numbers from 1 to 5 attached to the density profiles at an altitude of 1000 km and at the equatorial plane show corresponding regions in which the same ray paths traverse. And these numbers are also used in Figs. 6, 7, 8, 10 and 11 for the same purpose.

by multiplying the plasmapause model (AIKYO and ONDOH, 1971) by the following formula giving the latitudinal dependence of electron density.

$$N_L = 1 + \frac{B}{1+\exp\left(\frac{L-IR}{A}\right)},$$

where IR means the center location of ionospheric latitude gradient, and IR, A and B are taken to be 3.5, 0.05 and 2 respectively. By the multiplication with AIKYO and ONDOH model, the above density gradient is transferred to the plasmasphere along geomagnetic field lines, which results in an electron density decrease at $L=3.5$ in the equatorial plane like a plasmapause, whereas the plasmapause defined by AIKYO and ONDOH model is supposed to be located at $L=4.2$, and its effective half width is taken to be 0.2. The parameters used in the plasmasphere are as follows: Ion composition at the reference altitude of 1000 km is assumed to be $H^+=15.2\%$, $He^+=82.3\%$, $O^+=2.5\%$ and the electron density is 21000 el/cm^{-3}, and the temperature for ion and electron is assumed to be 1000 K.

With such a model, we calculated the ray paths from different entrance latitudes near Aldra to the southern hemisphere of the ISIS-II satellite. Figure 6 shows several ray paths from near Aldra to the ISIS-II located at 52.4° ($L=2.69$). In this figure, ray paths drawn by the dashed and the solid lines represent the positive and the negative doppler-shifted waves respectively, and the arrows denote their wave normal directions on the ray paths. Inner ($L=3.5$) and outer ($L=4.2$) dotted lines denote the location of the density gradients due to the ionospheric latitude gradient and plasmapause. For a wave starting at a latitude corresponding to the ionospheric latitude gradient, the ray is strongly bent inwards (SCARABUCCI, 1969). The rays injected from 60.3° and 57.7° (marked by a and b respectively at the starting latitude) encounter the gra-

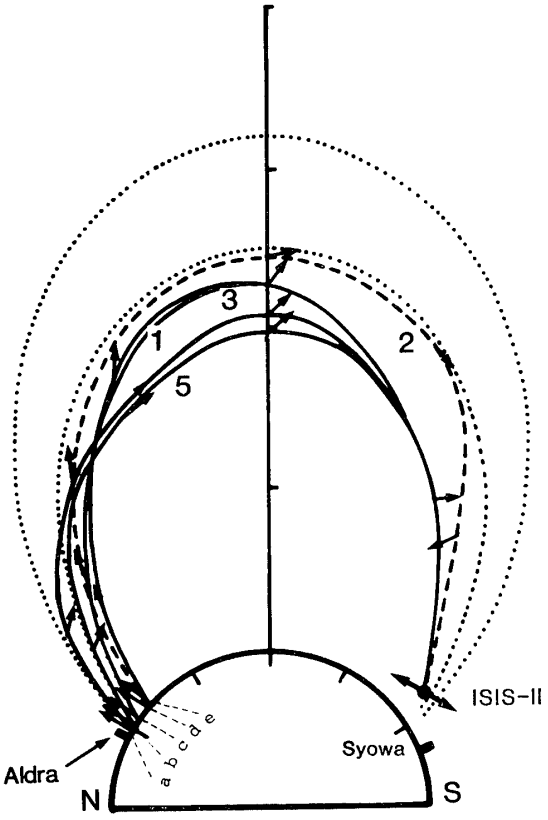

Fig. 6. Ray paths from Aldra in the northern hemisphere to the ISIS-II satellite in the southern hemisphere. These ray paths obtained by ray tracing are corresponding to five different doppler-shifted signals observed at $L=2.69$ as shown in Figs. 2, 4 and 6 respectively.

dients at $L=4.2$ and 3.5 where their wave normal directions are abruptly bent inwards (curve 5 in the figure). And as the waves propagate toward the inner magnetosphere where the spatial electron density gradient ($L<3.5$) is relatively small, the wave normal directions are gradually bent outward according to the magneto-ionic theory. Then, they come close to the resonance cone angle at the satellite locations in the conjugate hemisphere. As the waves entering from the lower latitude of 55.6° and 49.3° (c and e in Fig. 6) do not encounter either of the above two gradients in low altitude, the wave normal directions are gradually bent outwards. These signals which propagated to ISIS are observed as large negative doppler-shifted signals. On the other hand, when the rays encounter the inner density gradient in the southern hemisphere, the wave normals were abruptly bent inwards, and the rays were observed on the ISIS satellite as a slightly positive doppler-shifted signal. For example, a wave starting from 50.8° (d) propagates to a region above $L=3.5$ in the southern hemisphere, where the density gradient bends the wave normal inwards, and it can be observed as a slightly positive doppler-shifted signal. Thus, the signals which entered from different latitudes (a, b, c, d and e) into the magnetosphere were observed together by the ISIS satellite with different delay times.

Figure 7 shows the input magnetic latitude of the ray paths *versus* the output invariant latitude characteristic for an injected altitude of 130 km and an arrival altitude of 1400 km. The polarity of doppler shift is also shown by the solid and the dashed lines corresponding to the negative and the positive doppler branches respectively, and the numbers corresponding to these doppler branches are common with

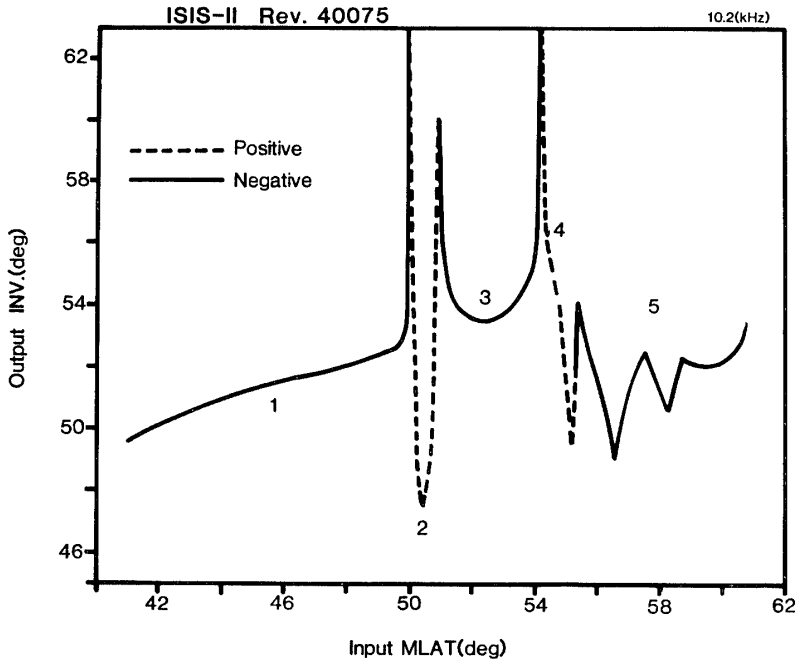

Fig. 7. Input (geomagnetic latitude)— output (invariant latitude) of the calculated ray paths for 10.2 kHz signals.

those indicated in Figs. 5, 6, 7, 8, 9 and 11.

In Fig. 8 the magnitude of the calculated doppler shift *versus* the arrival locations of the rays injected from different latitudes is shown. Namely, latitudinal or L dependence of the observed doppler shift envelope can be reproduced by the marked curves numbered by 1, 2, 3 and 4, and these envelopes are almost determined by the electron density distribution for $L<3.3$ as shown in Fig. 5. For starting L values from 3.3 to 4.2, the ray paths bent strongly inwards by the effects of both the ionospheric

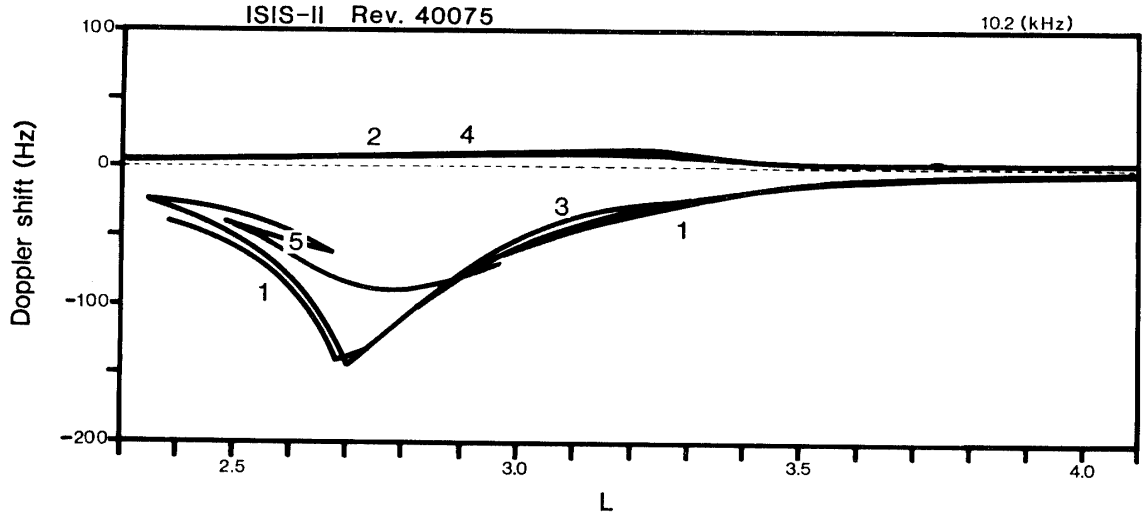

Fig. 8. Latitudinal variation of doppler shift frequency for 10.2 kHz signals calculated by ray tracing.

latitude gradient and plasmapause result in a medium amount of negative doppler shift, represented by the curve 5 in Fig. 8. Therefore, it is clear that density gradients in the ionosphere and magnetosphere produce medium negative doppler shift branches such as No. 5 inside the envelope indicated by Nos. 1, 2, 3 and 4 in Fig. 8, though it is not always enough to fill up the area inside the envelope.

On the other hand, measurement of the group delay time of the signal from the source to the satellites is also very important, because it provides us with a precious information of electron density on the ray paths. Figure 9 shows a relation between

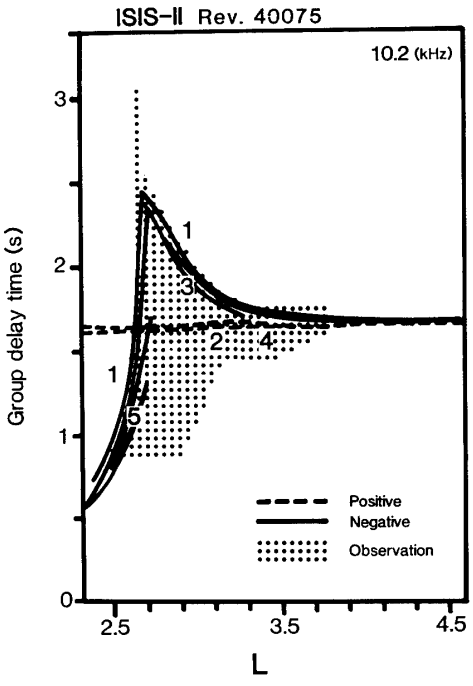

Fig. 9. A hatched area shows the latitudinal variation of measured group delay time of 10.2 kHz signals, and an area enclosed by the solid and the dashed lines shows those of calculated one.

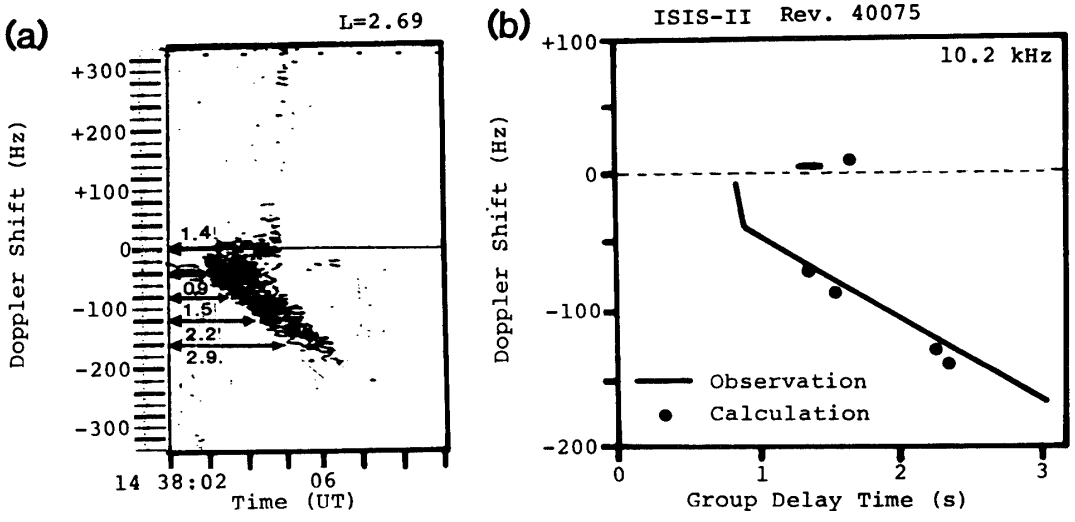

Fig. 10. (a) Spectrum of doppler-shifted 10.2 kHz signals observed at L=2.69.
(b) The observed (the solid line) and the computed (dot) spectral characteristics of doppler-shifted 10.2 kHz signals.

the group delay time and the arrival L shells of 10.2 kHz signals, and the solid and the dashed lines corresponding to the negative and the positive doppler-shifted signals respectively show the group delay time calculated by ray tracing. In this figure, a hatched area shows the latitudinal variation of measured group delay time, and a range of delay time at fixed ISIS locations implies that signals are composed of several different delay times (namely these are prolonged signals), and the measured delay time (hatched) shows a good agreement with those calculated (the solid and the dashed lines).

In Fig. 10a, the doppler shift and delay time characteristics for a 10.2 kHz signal actually observed at $L=2.69$ is shown, where the length of arrows denotes the group delay time from Aldra to ISIS-II. In Fig. 10b, the above characteristics are compared with those calculated (dots). It is evident from this figure that the obtained spectral characteristics were well reproduced.

Figure 11 shows the wave normal angles at the equatorial plane crossing for all ray paths which finally reach the satellite, *versus* L values of the satellite location. The solid and the dashed lines correspond to the negative and the positive doppler-shifted

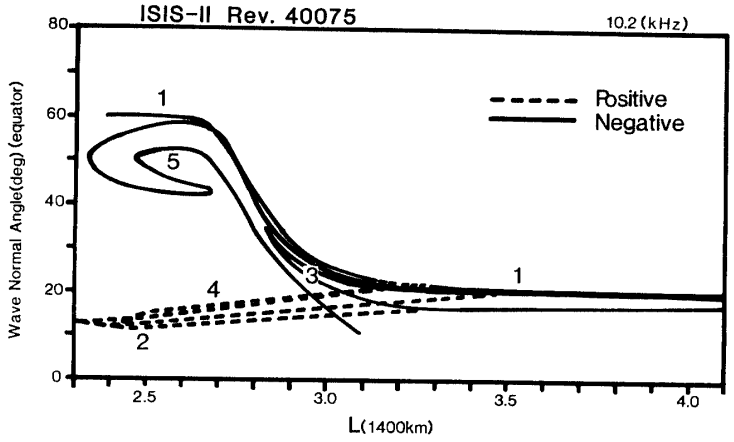

Fig. 11. ISIS-II satellite locations versus wave normal angles of the rays crossing the geomagnetic equator. Wave normal angles are greatly different between positive and negative doppler-shifted components, but this difference becomes small with increasing latitude.

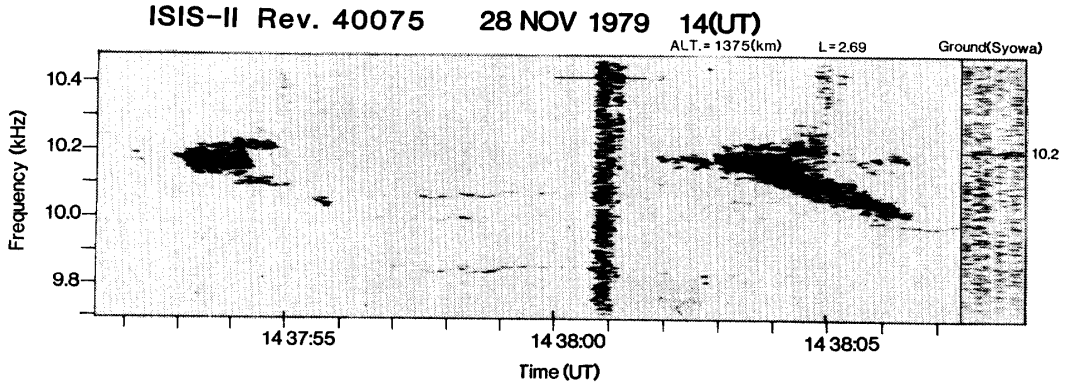

Fig. 12. Representative emissions triggered by slightly positive doppler-shifted 10.2 kHz signals, and no emissions triggered by the large negative doppler-shifted signals, $L=2.69$.

components respectively. Wave normal angles corresponding to negative doppler shift at the satellite (indicated by Nos. 1, 3 and 5 in Fig. 11) have a large angle at the equatorial plane, whereas those corresponding to positive doppler shift (2 and 4) have a small wave normal angle. As the emissions triggered by positively doppler-shifted signals were clearly observed for $2.6<L<2.8$ as shown in Fig. 12, their wave normal angles at the geomagnetic equatorial plane are estimated to be 10°–20° from Fig. 11. Moreover, as the emissions triggered by signals with positive and negative polarity of doppler shift are observed for $3<L<3.5$ (but this spectrum is not shown), it is clear from the figure that the wave normal angles of both components are within 10°–30°.

5. Examples of Emissions Triggered by Large Doppler-shifted Signals

A spectrogram indicated in Fig. 12 is a representative one which is triggered by slightly positive doppler-shifted signals. To the contrary, we have found several cases in which emissions were triggered by large doppler-shifted components. A spectrogram shown in Fig. 13 involves doppler-shifted 11.33 kHz signals with triggered emissions observed on December 17, 1979 by ISIS-II. The ISIS-II location at this data acquisition was around $L=2.7$ where the doppler shifts became maximum, therefore it is clearly seen that emissions is triggered by large negative doppler-shifted signals. Figure 14 also shows another example of emissions triggered by large negative doppler-shifted signals observed on the ISIS-II on December 28, 1980 from nearly $L=2.28$ to 2.55. In spite of the wide frequency (0–25 kHz) range spectrogram as shown in Fig. 14a, we can detect the fact that each spectrum of Omega signals (10.2 kHz) received during the interval from the beginning of data acquisition (0731: 35 UT) to nearly $L=2.52$ (0732: 45 UT) shows a slight negative frequency shift and prolongation of

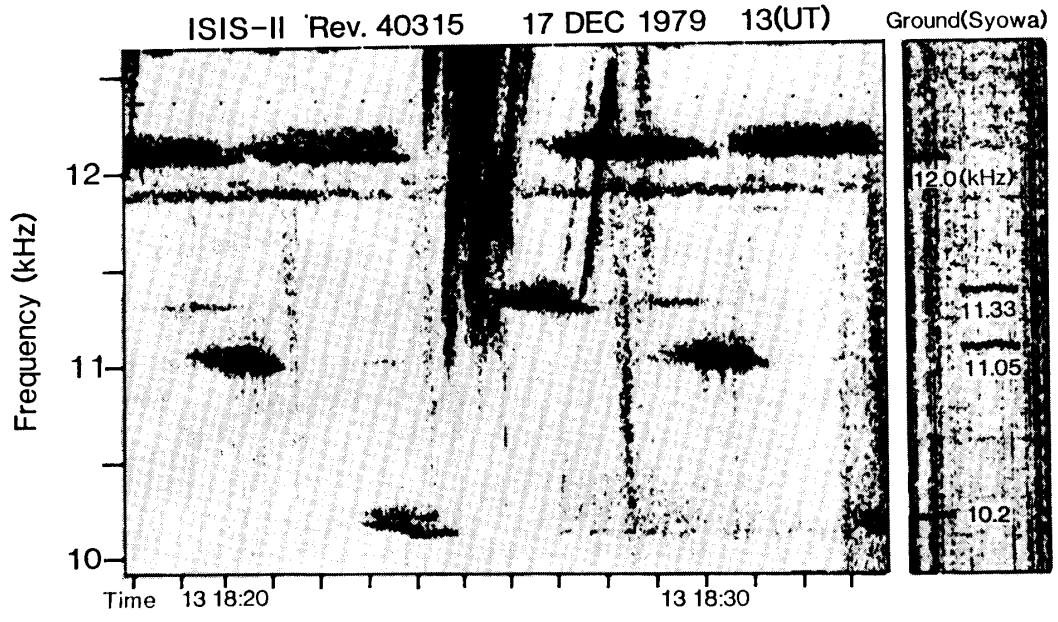

Fig. 13. Emissions triggered by large negative doppler-shifted 11.33 kHz signals observed on December 17, 1979.

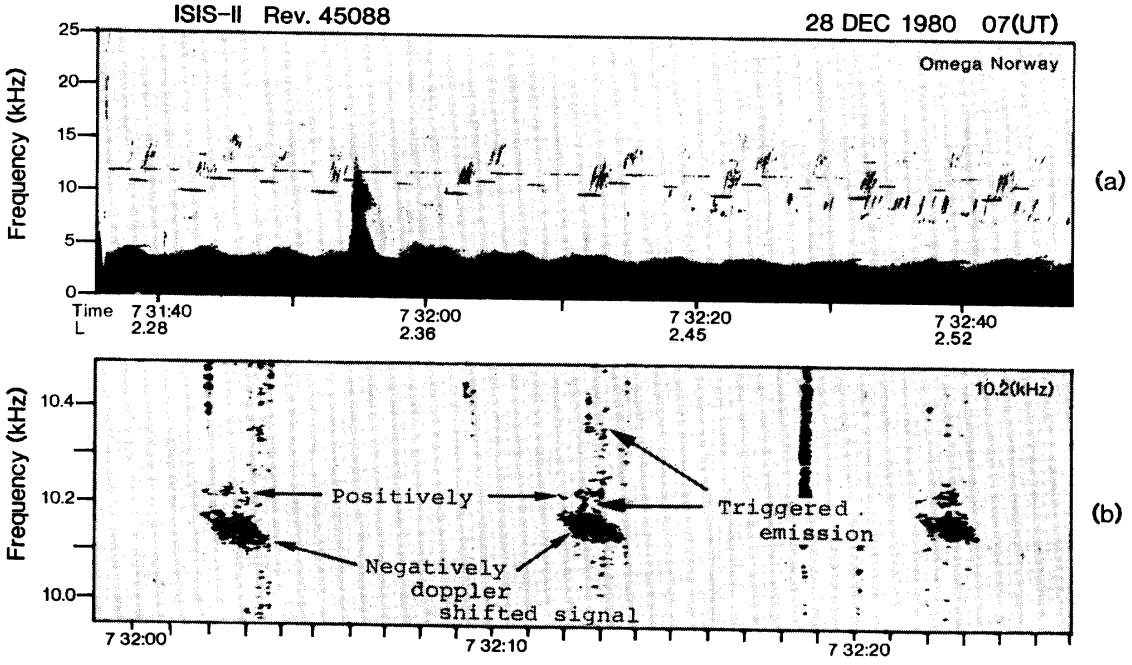

Fig. 14. (*a*) *Doppler-shifted signals and triggered emissions observed on December 28, 1980.* (*b*) *Expanded spectrogram of emissions triggered by large negative doppler shifted signals in the region of* $L<2.5$.

pulse length, which is a distinguished feature of the large negative doppler-shifted signals. Figure 14b indicates an expanded spectrogram in order to ascertain the above-mentioned evidences. It is found that the signal observed at 0732: 13 UT could be divided into two groups. One is a slightly positive doppler-shifted component and the other is a large negative doppler-shifted component. We can recognize that the emissions are triggered by the latter. The last example shown in Fig. 15a is emissions triggered by large positive doppler-shifted 13.6 kHz signals observed on ISIS-I satellite on December 11, 1979. Figure 15b is a frequency-time spectrogram exhibiting the latitudinal characteristics of doppler-shifted 13.6 kHz signals associated with triggered emissions, but, as it is not easy to distinguish the doppler-shifted signals from triggered emissions, latitudinal variations of doppler-shifted 11.05 kHz signals without emissions are shown in Fig. 15c. As ISIS-I moved in the opposite direction toward the equator from the high latitude as compared with the case indicated in Fig. 4, the latitudinal characteristics of doppler shift are of a reverse polarity as compared with Fig. 4. It is clear that the polarity of doppler shift is positive around the large dotted mark as shown in Fig. 15b, and emissions are triggered by these signals.

6. Summary and Conclusion

In the present paper, we have reported some examples of the triggering phenomena from which the wave normal angle of the triggering signal in the interaction region can be determined from their doppler frequency shift observed at the satellite. In order to clarify such latitudinal characteristics of doppler shift and the cause of prolongation, ray paths of injected signals starting from different latitudes at the iono-

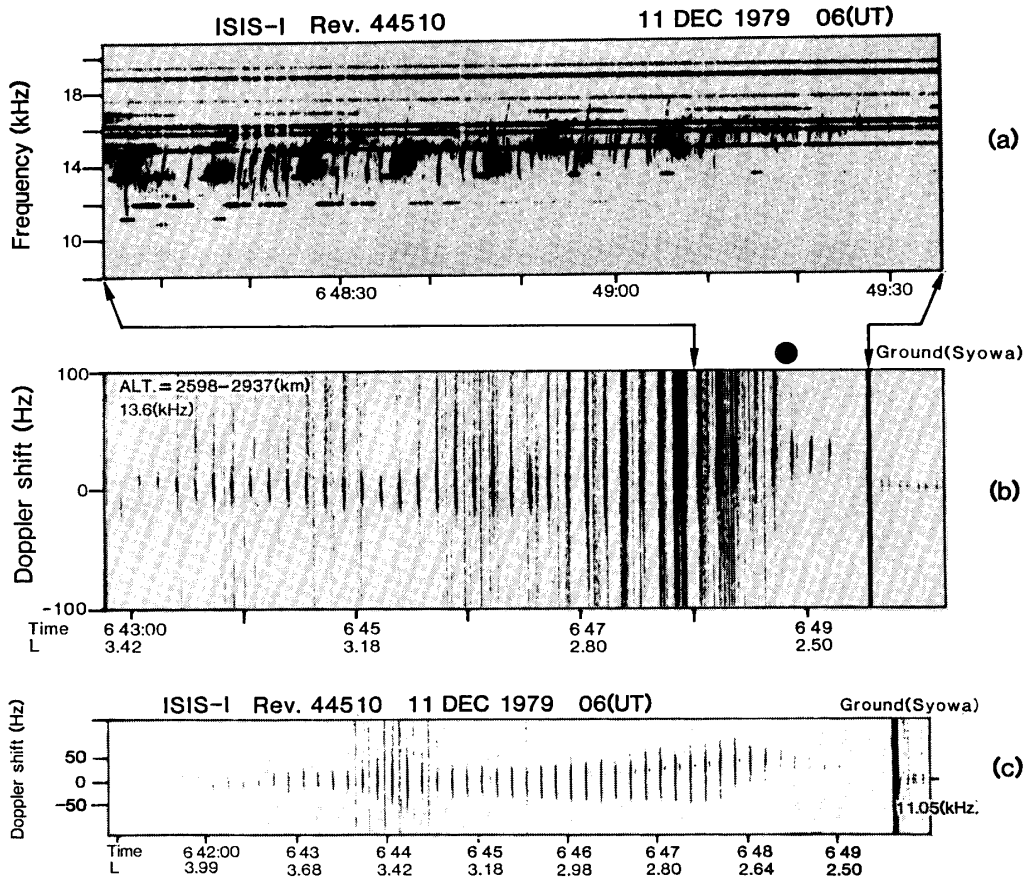

Fig. 15. (*a*) *VLF data observed by ISIS-I moving from the south pole to the equator.*
(*b*) *Doppler-shifted 13.6 kHz signals associated with triggered emissions.*
(*c*) *Latitudinal variation of the doppler shift for 11.05 kHz signals with opposite polarity compared with Fig. 4.*

spheric altitudes were calculated. If the latitudinal characteristics of the doppler shift actually observed as shown in Fig. 4 and the observed delay time of the signals can be reproduced by ray tracing, the electron density model used in the calculation may represent the actual electron density profile at the time of the ISIS observation. As shown in Fig. 8, the observed latitudinal characteristics of the doppler shift were reproduced by adopting an appropriate electron density profile in the ionosphere and magnetosphere, and it was found that sharp gradients of electron density profile due to a latitudinal ionospheric gradient as well as the plasmapause play an important role to produce the above doppler shift characteristics. AHMED *et al.* (1979) reported that middle latitude density gradient as well as trough corresponding to the base of plasmapause exists at the ISIS-I altitude of 2300–3600 km for $L>2$. However, unfortunately as the ISIS CEP (Cylindrical Electrostatic Probe) instrument to measure the electron density and temperature of the ionosphere in the vicinity of ISIS satellites was not operated normally during the period of our satellite tracking (MIYAOKA, private communication, 1983), we have not obtained the electron density data to ensure the assumed density model as shown in Fig. 5. If there is no existence of the mag-

netospheric density gradient located at $L=3.5$, it is clear that the latitudinal variations of doppler shift and the group delay time must be greatly different from those of observed data. As shown in Fig. 11, the wave normal angle is less than 30° for the dashed line (positive doppler shift), and is 30°–60° for the negatively doppler-shifted signals, especially the latter is confined within the range of 40°–60° for $L<2.7$. As the magnitude and the polarity of doppler shift have not always remarkably changed every VLF data used in this paper, most of the transmitter signals have shown similar latitudinal characteristics of doppler shift as shown in Figs. 4 and 14a. The wave normal angles in the equatorial interaction region for large doppler-shifted Norway Omega signals ranged from 40° to 60°, irrespective of the direction of the satellite trajectories as shown in Figs. 13, 14 and 15. The condition of these propagations is evidently "non-ducted". Recently BELL (1984) presented a theory of the nonlinear gyroresonance interactions between energetic electron and coherent VLF waves propagating in the whistler mode at an arbitrary angle of wave normal with respect to B_0, and concluded that near the geomagnetic equator where the generation region is believed to exist, a gradient of wave normal angle may play a very important role in the phase trapping process for non-ducted waves.

Our observational results of propagation characteristics of Norway Omega signal in the equatorial interaction region will provide an important information on the mechanisms of oblique wave particle interactions.

Acknowledgments

It is our pleasure to acknowledge all members of the 17th–22nd wintering parties of Japanese Antarctic Research Expedition for their efforts in the ISIS telemetry reception and various ground observations at Syowa Station, Antarctica. We wish to thank Prof. T. HIRASAWA of National Institute of Polar Research for his encouragement and kind suggestions to our work. Our thanks are extended to Drs. R. E. BARRINGTON, N. MATSUURA, T. ONDOH, CRC ISIS working group and NASA for their kind supports to the telemetry reception of the ISIS-I and ISIS-II data at Syowa Station. This work has been conducted through the joint research with National Institute of Polar Research, and has been supported by Grant in Aid for Science Research Project No. 58460047 by the Ministry of Education, Science and Culture in Japan.

References

AHMED, M., SAGALYN, R. C., WILDMAN, P. J. L. and BURKE, W. J. (1979): Topside ionospheric trough morphology; Occurrence frequency and diurnal, seasonal, and altitude variations. J. Geophys. Res., **84**, 489–498.

AIKYO, K. and ONDOH, T. (1971): Propagation of nonducted VLF waves in the vicinity of the plasmapause. J. Radio Res., **18**, 153–181.

BELL, T. T. (1984): The nonlinear gyroresonance interactions between energetic electrons and coherent VLF waves propagating at an arbitrary angle with respect to the Earth's magnetic field. J. Geophys. Res., **89**, 905–918.

BELL, T. F., INAN, U. S. and HELLIWELL, R. A. (1981): Nonducted coherent VLF waves and associated triggered emissions observed on the ISEE-1 satellite. J. Geophys. Res., **86**, 4649–

4670.

CARPENTER, D. L. and MILLER, T. R. (1976): Ducted magnetospheric propagation of signals from the Siple, Antarctica, VLF transmitter. J. Geophys. Res., **81**, 2692–2700.

CARPENTER, D. L., STONE, K. and LASCH, S. (1969): A case of artificially triggering of VLF magnetospheric noise during the drift of a whistler duct across magnetic shells. J. Geophys. Res., **74**, 1848–1855.

CERISIER, J. C. (1973): A theoretical and experimental study of non-ducted VLF waves after propagation through the magnetosphere. J. Atmos. Terr. Phys., **35**, 77–94.

CERISIER, J. C. (1974): Ducted and partly ducted propagation of VLF waves through the magnetosphere. J. Atmos. Terr. Phys., **36**, 1443–1467.

EDGAR, B. C. (1976): Theory of VLF doppler signatures and their relation to magnetospheric density structure. J. Geophys. Res., **81**, 3327–3339.

HELLIWELL, R. A. (1967): A theory of discrete VLF emissions from the magnetosphere. J. Geophys. Res., **72**, 4773–4790.

HELLIWELL, R. A. and KATSUFRAKIS, J. P. (1974): VLF waves injection into the magnetosphere from Siple Station, Antarctica. J. Geophys. Res., **79**, 2511–2518.

KIMURA, I. (1966): Effects of ions on whistler mode ray tracing. Radio Sci., **1**, 269–283.

KOONS, H. C., EDGAR, B. C., DOWDEN, R. L., CARRINGTON, C. G. and AMON, E. S. (1974): Multipath doppler shift in man-made VLF signals. ELF-VLF Radio Wave Propagation, ed. by J. A. HOLTET. Dordrecht, Reidel, 311–316.

LEFEUVRE, F., NEUBERT, T. and PARROT, M. (1982): Wave normal directions and wave distribution functions for ground-based transmitter signals observed on GEOS-1. J. Geophys. Res., **87**, 6203–6217.

MATSUO, T., KIMURA, I. and YAMAGISHI, H. (1983): Statistical feature of non-ducted signal and associated ASE observed by ISIS-I and -II satellites. Mem. Natl Inst. Polar Res., Spec. Issue, **26**, 103–112.

NEUBERT, T., UNGSTRAP, E. and BAHNSEN, A. (1983): Observations on the GEOS-1 satellite of whistler mode signals transmitted by the Omega navigation system transmitter in northern Norway. J. Geophys. Res., **88**, 4015–4025.

SCARABUCCI, R. R. (1969): Interpretation of VLF signals observed on the OGO-4 satellite. Tech. Rep. No. 3418-2, Stanford, Radio Sci. Lab., Stanford Univ.

WALTER, F. and ANGERAMI, J. J. (1969): Nonducted mode of VLF propagation between conjugate hemisphere; Observations on OGO's 2 and 4 of the 'Walking-Trace' whistler and of doppler shifts in fixed frequency transmissions. J. Geophys. Res., **74**, 6352–6370.

(Received August 27, 1984; Revised manuscript received December 5, 1984)